June 19, 2017

Computational Study of MoS2/HfO2 Defective Interfaces for Nanometer-Scale Electronics

Santosh KC, *University of Texas at Dallas*
Roberto C. Longo, *The University of Texas at Dallas*
Robert M. Wallace, *University of Texas at Dallas*
Kyeongjae Cho, *The University of Texas at Dallas*

ACS OMEGA

Article

http://pubs.acs.org/journal/acsodf

Computational Study of MoS_2/HfO_2 Defective Interfaces for Nanometer-Scale Electronics

Santosh KC,[†,‡] Roberto C. Longo,[*,†] Robert M. Wallace,[†] and Kyeongjae Cho[*,†]

[†]Department of Materials Science & Engineering, The University of Texas at Dallas, 800 W. Campbell Road, Richardson, Texas 75080, United States

[‡]Materials Science and Technology Division, Oak Ridge National Lab, 1 Bethel Valley Road, Oak Ridge, Tennessee 37831, United States

Supporting Information

ABSTRACT: Atomic structures and electronic properties of MoS_2/HfO_2 defective interfaces are investigated extensively for future field-effect transistor device applications. To mimic the atomic layer deposition growth under ambient conditions, the impact of interfacial oxygen concentration on the MoS_2/HfO_2 interface electronic structure is examined. Then, the effect on band offsets (BOs) and the thermodynamic stability of those interfaces is investigated and compared with available relevant experimental data. Our results show that the BOs can be modified up to 2 eV by tuning the oxygen content through, for example, the relative partial pressure. Interfaces with hydrogen impurities as well as various structural disorders were also considered, leading to different behaviors, such as n-type doping, or introducing defect states close to the Fermi level because of the formation of hydroxyl groups. Then, our results indicate that for a well-prepared interface the electronic device performance should be better than that of other interfaces, such as III−V/high-κ, because of the absence of interface defect states. However, any unpassivated defects, if present during oxide growth, strongly affect the subsequent electronic properties of the interface. The unique electronic properties of monolayer-to-few-layered transition-metal dichalcogenides and dielectric interfaces are described in detail for the first time, showing the promising interfacial characteristics for future transistor technology.

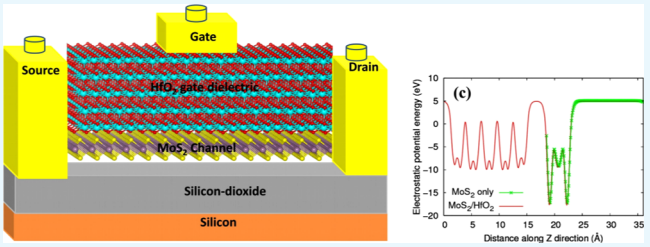

1. INTRODUCTION

For the development of future metal−oxide field-effect transistors (MOSFETs), the conventional silicon transistor channel, which has already reached its physical limit of scaling, has to be replaced by an alternative material with higher carrier mobility[1] and a high-κ dielectric, providing a higher gate capacitance for thicker films. For this purpose, III−V semiconductors, which provide high electron and hole drift mobilities, have been studied extensively.[1−3] The detailed interfacial oxidation mechanism of Si and SiO_2 has been studied from first-principles molecular dynamics simulations, which explained a scheme that allows for strain relief during growth, resulting in a high-quality interface.[4] It was also evidenced by the very low density of defects observed at this interface (less than 1 per 10^4 interface atoms).[5]

To be a suitable candidate for use in future field-effect devices, the material should be thermodynamically stable with the corresponding high-κ oxide as well as able to unpin the Fermi level with minimal defect trap density (D_{it}). Silicon dioxide has been the dielectric of choice for many field-effect devices, and, if the present miniaturization trends continue, the projected oxide thickness should be less than 1 nm, or about five silicon atoms across.[6]

To date, many studies have been focused on using hafnium dioxide (HfO_2)-based dielectrics because of their high dielectric constant (~20), thermal stability, and sufficient band offsets (BOs). Despite the enormous effort to realize a low D_{it} III−V/high-κ interface, these materials continue to suffer from high defect densities, leading to threshold voltage shifts, large leakage current, and charge trapping, thus causing instability of the device. The nature and origin of the defects at the interface continues to be investigated to optimize the oxide growth deposition conditions and adopt a suitable defect passivation mechanism.[7,8] Recently, there has been substantial interest on two-dimensional (2D) materials (such as graphene[9−11]) for electronic device applications because of their higher carrier mobilities and interfaces devoid of defect states. However, owing to the intrinsic zero band gap at the Dirac point, graphene-based layered FETs suffer from high leakage currents. In addition, tuning the band gap of graphene is not feasible, which limits its potential applications,[12,13] although there has been a recent report on the realization of a single-layer graphene p−n junction, in which the carrier type and density in two adjacent regions were locally controlled by electrostatic gating, opening new techniques for a future graphene-based bipolar technology.[14] Therefore, because of the several

Received: May 19, 2017
Accepted: June 1, 2017
Published: June 19, 2017

DOI: 10.1021/acsomega.7b00636
ACS Omega 2017, 2, 2827−2834

aforementioned limitations, the semiconductor device community has turned its attention to other 2D or binary quasi-2D materials beyond graphene, searching for unique electronic, optical, chemical, and mechanical properties for a wide range of future applications. Among these, transition-metal dichalcogenides (TMDs), well known for being used as lubricant additives or coating materials because of their interesting tribological properties,[15−17] have attracted remarkable interest for device applications. The unique physical properties of semiconducting TMDs, due to their crystal structure, symmetry, and thickness (with changes in the interlayer coupling and strain- and field-dependent modulation of the electronic properties, including the effects of quantum confinement), enhance their tunabilty and thus make TMDs promising device materials.[18,19]

TMDs have a layered bulk structure that can be exfoliated into a single-layer semiconducting 2D material with sizable band gaps or metallic behavior, depending on the type of metal−chalcogen combination.[20−26] Ideally, these materials are anticipated to have a low D_{it}, as the dangling-bond density should be minimal. They have been obtained by mechanical or chemical exfoliation as well as chemical vapor deposition techniques.[12,27−31] Two-dimensional MoS_2 has been recently investigated for electronic device applications, showing promising features of a high ON−OFF current ratio (10^8), an appreciable carrier mobility (~200 $cm^2/V{\cdot}s$),[12] and a higher current density[32,33] with a high-κ gate dielectric. Using a scandium electrode, the carrier mobility can be further enhanced to ~700 $cm^2/V{\cdot}s$, suggesting a negligible Schottky barrier at the MoS_2/Sc interface.[34] However, most of the metal contacts on single-layer MoS_2 show the well-known problem of Fermi-level pinning mechanism,[35,36] whereas the metal/oxide interface seems to be more promising. Although initial reports show mobilities in the range of 0.1−10 $cm^2/V{\cdot}s$ for exfoliated monolayer MoS_2 on SiO_2,[9] a recent study claims additional mobility enhancement by reducing the impurity scattering by high-κ deposition.[37] Moreover, quantum transport simulations of an ideal TMD device indicate that monolayer MoS_2 MOSFETs with HfO_2 can achieve near-ideal subthreshold slope, suppression of drain-induced barrier lowering, and gate-induced drain leakage.[38] The switching behavior of a TMD transistor degrades significantly with thicker layers due to diminished gate control. Monolayer TMDs show the best scalability with the largest ON−OFF ratios, achieving ON current levels of 450 $\mu A/\mu m$ for an ON−OFF ratio of 10^5, whereas the bilayer devices deliver about half of this value exhibiting significant loss of gate control upon addition of an extra layer to the conducting channel.[39] The literature lacks a detailed, atomic-level investigation of the nature of TMD/high-κ dielectrics interface. For a detailed understanding and further optimization of TMD-based electronic devices, it is important to examine in detail the atomic and electronic structures of TMD/HfO_2 interfaces under different growth conditions.

Here, a lattice-matched monolayer of the MoS_2/HfO_2 interface model is developed and the interface atomic structures and the corresponding electronic properties are investigated using density functional theory (DFT) calculations at different levels of accuracy. The model interface is extensively investigated as a function of oxygen and hydrogen incorporation, representing different HfO_2 atomic layer deposition (ALD) growth conditions on MoS_2. The DFT results are compared with previously reported experimental values from in situ X-ray photoelectron spectroscopy (XPS) studies of HfO_2 ALD on bulk MoS_2.[40] Moreover, we also investigate the influence of several structural defects and disorders at the interface on the electronic properties. These studies on MoS_2/HfO_2 can be extended to other TMDs and high-κ oxides in an effort to identify the most promising device material candidates, which might improve the performance of MoS_2 as a device channel material.

2. RESULTS AND DISCUSSION

First, we optimized the atomic structure of the stoichiometric MoS_2/HfO_2 interface model and analyzed its electronic structure. Then, the oxygen concentration at the interface is varied to investigate the impact on the electronic properties of the interface. Figure 1c shows the variation of electrostatic

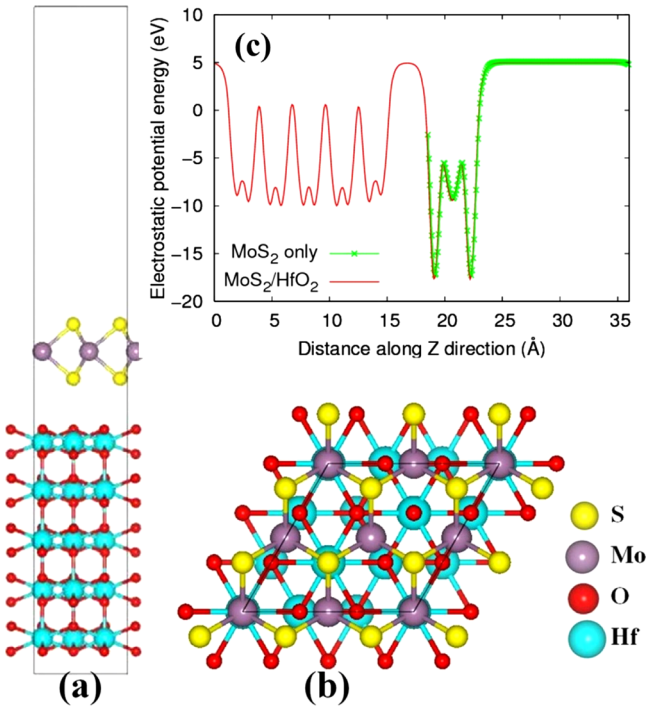

Figure 1. Atomic structure of the MoS_2/HfO_2 interface: (a) side view and (b) top view of the interface. Hafnium, oxygen, molybdenum, and sulfur are represented by turquoise, red, purple, and yellow spheres, respectively. (c) Electrostatic potential profile perpendicular to the interface area (along the z-direction). The red lines represent the variation of interfacial potential, whereas the green line shows the contribution of the isolated MoS_2 monolayer. Both potentials are measured with respect to the E_{VBM}.

potential along a direction perpendicular to the interface area of the model. The vacuum level is flat, indicating that there is no electrostatic polarization (no significant charge transfer) caused by HfO_2 deposition on the MoS_2 layer. This finding indicates that there is a very weak van der Waals interaction between the MoS_2 monolayer and HfO_2. This is consistent with a recent experimental study on the ALD of HfO_2 on the MoS_2 surface, where no covalent bonding between the HfO_2 and MoS_2 layers was detected.[40] Symmetric potential profiles are observed for the MoS_2 monolayer and HfO_2.

To understand the electronic properties and to obtain the BOs between MoS_2 and HfO_2 across the interface, the local density of states (DOS) at bulklike Hf, O, Mo, and S atoms away from the interface is computed. The computed band gaps of HfO_2 are 4 and 6 eV, as obtained with generalized gradient approximation (GGA) and Heyd, Scuseria, and Ernzerhof

DOI: 10.1021/acsomega.7b00636
ACS Omega 2017, 2, 2827−2834

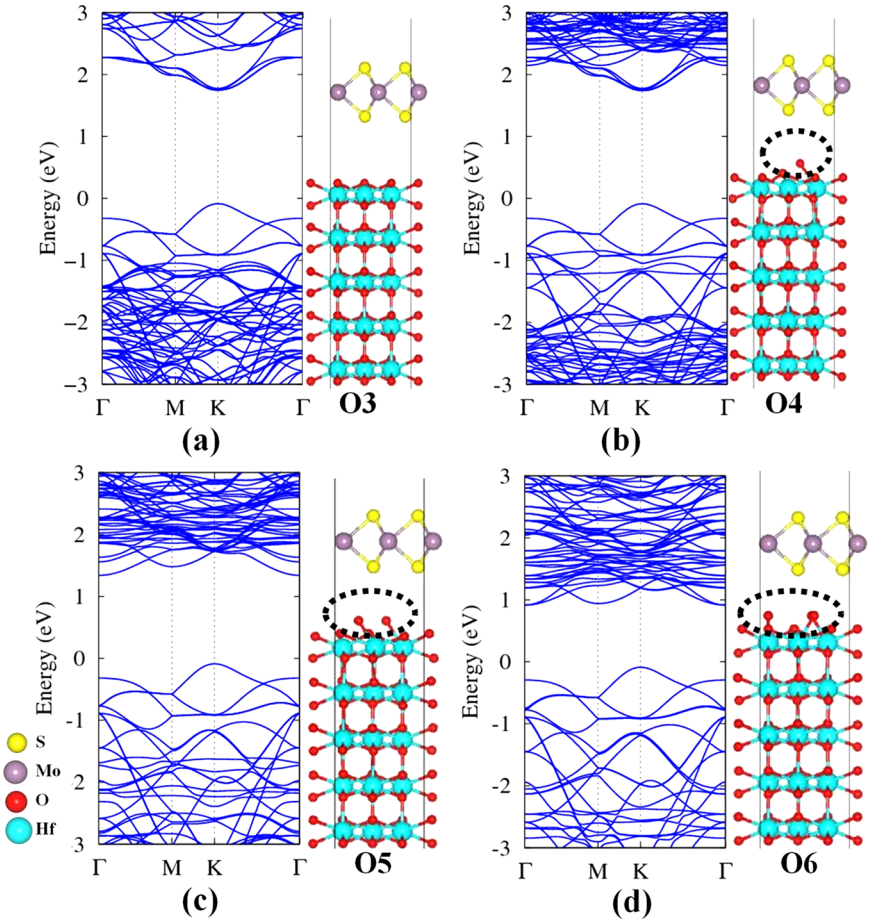

Figure 2. Electronic band structures of MoS_2/HfO_2 interfaces with various oxygen concentrations at the interface: (a) Three interfacial oxygen atoms (O3), (b) O4, (c) O5, and (d) O6. The zero of the energy is aligned to the Fermi level. The atomic structure of the MoS_2/HfO_2 interfaces with various oxygen contents at the interface is also shown. Hafnium, oxygen, molybdenum, and sulfur are represented by turquoise, red, purple, and yellow spheres, respectively.

(HSE) calculations, respectively (cf. with the experimental result of 5.9 eV[40]). For the MoS_2/HfO_2 interface, GGA calculations yield a band gap of 1.8 eV, whereas HSE results widen the gap to 2.34 eV. Then, even though the HSE band gap of HfO_2 matches the experimental result much better than the GGA band gap, qualitatively the BOs of the interface remain relatively unchanged. Moreover, a trend of band gap decrease when going from single to multilayer MoS_2 is observed, with significant changes in the BOs (as will be discussed later).

Valence band offset (VBO) and conduction band offset (CBO) obtained from GGA calculations are ∼1.0 and ∼1.24 eV, respectively, whereas those obtained from HSE calculations are ∼1.60 and ∼2.0 eV, respectively (Figure S1), and the corresponding experimental values for the bulk interface are ∼2.67 and ∼2.09 eV (E_g = 1.23 eV for the bulk).[40] These results show that qualitatively and quantitatively the BOs are large enough to avoid leakage current during the electronic device operation, although the calculations are for a single MoS_2 monolayer; whereas the available experimental values were obtained for bulk MoS_2/HfO_2 interface (the changes in the band gap with interface thickness will be discussed later).

To mimic the oxidizing environment of the ALD process and to model the experimental conditions in a more realistic manner, the interfacial oxygen concentration is varied and the effect on the electronic properties is investigated. Our calculations show strong effects of the interfacial oxygen content on the electronic structure of the interface and the corresponding BOs. Figure 2 shows the atomic structures of the MoS_2/HfO_2 interface with different amounts of oxygen concentration (O6 refers to six interfacial O atoms, corresponding to a high oxygen concentration (1.76×10^{15} O atoms/cm^2), and O3 refers to the lower limit of three interfacial O atoms (0.88×10^{15} O atoms/cm^2) within the supercell of the interface model). Then, the electronic band structures of those interfaces are investigated to elucidate the impact of the oxygen concentration on the properties of the interface. Figure 2a–d shows the band structures of the MoS_2/HfO_2 interface with different oxygen concentrations at the interface, with Table S1 summarizing the numerical results. For device applications, the evaluation of the BOs between MoS_2 and HfO_2 as a function of the oxygen concentration is very important, as they are one of the key parameters that reflect the quantum mechanical electron tunneling mechanism across the interface. From the analysis of the variation of the potential across the interface in the previous section, there is no significant charge transfer for the stoichiometric interface. In the absence of charge transfer, the BOs are obtained by the electron affinity (EA) rule or Anderson's rule.[41] In our model, the change of the interfacial oxygen concentration directly affects the EA. For instance, for the O3 model, the VBO is always larger than 1 eV (1.8 eV), at the GGA (HSE) level of

DOI: 10.1021/acsomega.7b00636
ACS Omega 2017, 2, 2827−2834

approximation, and it increases with O concentration at the interface.

A change in the O concentration at the interface affects the edge states of HfO_2, but not MoS_2, because the valence band maximum (VBM) of HfO_2 is dominated by O 2p states. A higher O concentration shifts down the VB edge of HfO_2 due to the O 2p redistribution at the VBM.[42,43] As a consequence, the VBO increases with the amount of interfacial oxygen. Thus, the VBO can be controlled by varying the oxygen concentration, a property directly related to the ambient atmospheric oxygen pressure during the oxide formation.

By controlling the interfacial O concentration gradually, the VBOs can be modified up to 1.8 eV (O3 = 1.0 eV; O4 = 1.8 eV; O5 = 2.3 eV; and O6 = 2.8 eV) at the GGA level of calculation, although a significant reduction of the CBO is also observed for higher oxygen concentrations (see Supporting Information). This variation of the BOs will significantly affect the device performance. However, the trend showing a bang gap narrowing with the increase of oxygen concentration remains unchanged. Moreover, we have identified for the very first time the unique nature of the electronic properties of few-layered TMD/HfO_2 interfaces, by showing the nonidentical behavior of each TMD individual layer, even for stoichiometric interfaces, which opens a new possibility of multiconducting channel concept for FET devices (Figure 3): when going from single-layer to multilayer MoS_2, the electronic properties of the interface are modified, as the layers are coupled with van der Waals forces through a weak interaction between S p_z states. Approximately, the middle MoS_2 layers control the electronic band edges. Thus, this unique feature of TMDs shows novel implications for possible TMD-based devices. Moreover, doping or oxidation will change the top and bottom layers interfaced with the high-κ dielectric, whereas the layers beneath will be physically intact, with only the electronic structure altered, thus showing new and unique functionalities. The layer-projected DOS (Figure 3) confirms that the individual layers are not identical in terms of their electronic structure, affecting the BOs and the band gaps. This finding emphasizes the unique characteristics of hypothetical TMD-based devices compared to those of standard Si- or III−V-based electronics.

Besides oxygen impurities, hydrogen impurities strongly alter the structural and electronic properties of different host materials into which they are incorporated, affecting the performance of the electronic devices. During the ALD growth process, the use of water as an oxygen precursor can provide hydrogen species in the semiconductor surface. Defect (dangling bond) passivating effects or dopant passivation behavior are well known in conventional semiconductors. Here, the presence of H atoms at the interface at several oxygen concentrations is also examined (Figure S2). Our results show that for the O3 model an additional H impurity results in n-type doping behavior, as can be seen from the shifting of the Fermi level up to the conduction band in the band structure diagram shown in Figure S2a. However, for the O6 model, the H impurity forms an OH bond, inducing defect states close to the Fermi level. Then, both H and OH at the interface show a strong impact on the electronic properties of the interface. Additionally, OH-like species present at the interface shift the Fermi level toward the valance band edge and exhibit p-type doping behavior and gap states (which can be potentially harmful for device applications due to Fermi-level pinning or charge transfer to/from the defect state), as observed in Figure S3. It is worthwhile to note that OH species are expected to be

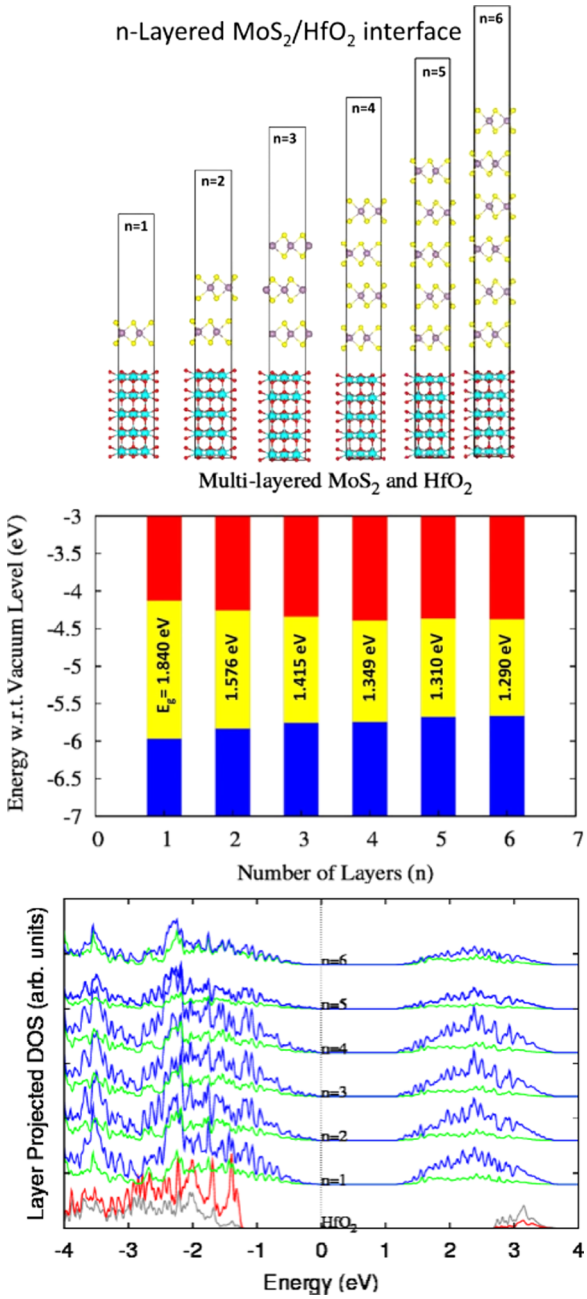

Figure 3. Atomic structures of multilayered MoS_2/HfO_2 interfaces (upper panel); electronic band gap variation (the energy values are referred to the vacuum level) (middle panel); and layer-projected DOS (lower panel).

abundant in a standard ALD process. The incorporation of an H impurity (0.88×10^{15} H atoms/cm^2) on the stoichiometric interface model causes a defect-state density of about 1.5×10^{14}/eV·cm^2 close to the band edges.

Interface structural disorder originated during the growth process also affects the electronic properties and the thermodynamic stability of the resulting device. Here, several likely defective interfaces (Figure S4) are proposed to investigate how the electronic properties are affected by different atomic arrangements. The notation O6−O−S refers to a modified O6 interface model in which oxygen from HfO_2 is interchanged with S from the MoS_2 side, as shown in Figure S4a, along with the corresponding electronic band structures

DOI: 10.1021/acsomega.7b00636
ACS Omega 2017, 2, 2827−2834

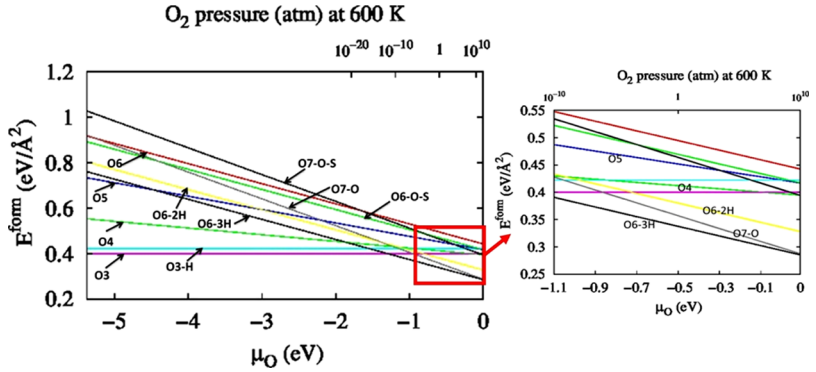

Figure 4. Thermodynamic stability of the MoS_2/HfO_2 system with interfacial impurities. The interface formation energy is given with respect to the oxygen chemical potential in the following range: -5.38 eV $\leq \mu_O \leq 0$ eV (setting the bulk value to zero). The right plot is a zoom of the section corresponding to experimental conditions around 1 atm.

showing additional bands inside the gap of MoS_2. The notation O7−O−S refers to an interface in which the bottom sulfur atoms of MoS_2 are completely replaced by O atoms and the interfacial O atoms of HfO_2 are bonded with S atoms, as shown in Figure S4b. It can be seen that these interchange defects caused interface defect states in the band gap of MoS_2 between 1.2 and 1.5 × 10^{14}/eV·cm^2, for a defect density of about 1 × 10^{15} O or H atoms/cm^2.

Defect-state generation can be anticipated if there is S and O bonding at the interface or in the TMD surface.[44,45] S and O interchange to form Mo−O and S−O bonds, reducing the band gap significantly. In pristine MoS_2, the main VBM contribution comes from the hybridization of Mo d and S p orbitals, whereas CBM is mainly composed of Mo d orbitals. In the disordered system, the hybridization is weakened due to rehybridization at the interface, inducing gap states in the band gap of MoS_2. Thus, with extrinsic defects present at the interface, gap states will be induced, resulting in a deleterious impact on the device performance. The band structure depicted in Figure S4c of a single S−Mo−O layer with HfO_2 (Supporting Information) shows that the band gap narrows substantially, indicating a metallic character (MoO_2 is a metal[46]). The metallic nature of the contact also indicates the possibility of utilizing such interface to make contact materials for future TMD-based devices.[47]

To determine the thermodynamic stability of the different interface models, we investigate their formation energies (see Supporting Information for details) as a function of the oxygen chemical potential (μ_O), as shown in Figure 4. The formation energy increases gradually when the oxygen chemical potential changes from O-rich to O-poor limit, for the O6 to O3 interface models considered in this study, with the oxygen-rich environment being thermodynamically favorable.

Figure 4 also shows that the thermodynamic stability of the O3 model is higher than that of O4, O5, and O6 models for a wide range of chemical potentials, albeit far from realistic ALD conditions. The relative formation energy of the O6−3H defect model is relatively low in the range close to a partial pressure of 1 atm, showing that it is stable in O-rich environments. Besides, as can be seen in Figure S2f, OH species formed at the interface passivate all of the oxygen dangling bonds. Because of that, the local atomic structure is distorted compared to that of the pristine interface model, also inducing a slight distortion in the layers underneath. The stability of the O3−H model is lower than that of the O3 model, which means that for a stoichiometric interface, H impurities increase the formation energy. However, the O7−O−S model is the least stable among all of the interface models investigated but O7−O is stable under O-rich conditions. This thermodynamic analysis indicates that most of the defective surfaces are less likely to be formed. However, on the contrary, additional hydrogen impurities at the interface are more likely to be formed compared to that in the stoichiometic MoS_2/HfO_2 interface (O3 model).

The study of the effect of oxygen concentration on the electronic structure has been reported previously for III−V/high-κ interfaces.[43] It was shown that the most stable interface corresponds to a high concentration of oxygen and that the VBOs can be modified up to ∼2 eV by decreasing the interfacial oxygen content. However, although from different nature, there are always gap states, due to the presence of dangling bonds on the III−V semiconductor surface. On the contrary, the inert nature of TMD monolayers does not induce interfacial gap states, which can in turn arise from surface defects formed during their synthesis. Our results have shown that postprocessing could aim to remove or passivate such defects, thus increasing carrier mobility.[48] Also, nonstoichiometric interfaces can also behave as contacts, exhibiting an Ohmic electrical behavior.[49] Interface defect states will affect the carrier mobility in the electronic device because they act as charge traps. Indeed, high-density interface states can cause issues such as frequency dispersion of capacitance, Fermi-level pinning, low electron mobility, or instability of device operations.[50] In this study, we have identified the preferable interface structures for specific chemical environments. Such chemical environment can be monitored and/or controlled through the oxygen partial pressure. Then, the obtained VBOs for the different interface structures show the dependence of the BOs and band gaps (which are easily measurable) on each specific interface structure. Therefore, finally, one can easily correlate experimentally measured data with defective interfaces, identifying the origin of any possible defect and/or impurities.

Besides, in electronic devices such as FETs, the gate field controls the overall operation of the device, by sweeping the Fermi level across the semiconductor band gap to change the carrier density in the channel material. However, a significant interface-state density within the semiconductor band gap can pin the Fermi level to those gap states, which will ultimately compromise the efficiency of the gate field control of the transistor. As it has already been shown that a high density of interface states is the primary cause for the poor device

DOI: 10.1021/acsomega.7b00636
ACS Omega 2017, 2, 2827−2834

performance of III−V/dielectric interfaces, the analysis of possible defect states and their origin for TMD and high-κ dielectric interfaces becomes crucial to prevent poor device performance, highlighting again the importance of defect passivation or preparing defect-free interfaces.

3. CONCLUSIONS

In conclusion, in this study, we have shown that the BOs of MoS_2/HfO_2 interfaces change with increasing interfacial oxygen content, indicating their dependence on the oxide growth environment. For the stoichiometric, defect-free MoS_2/HfO_2 interface, no charge transfer between HfO_2 and MoS_2 is observed. However, disorder and defects at the interface can introduce gap states, which would be harmful for device applications due to the subsequent charge transfer or Fermi-level pinning. Thus, the interfacial oxygen content significantly affects the thermodynamic stability and the BOs of the interface. Furthermore, interfacial hydrogen impurities are also shown to have a strong effect on the interfacial stability and the corresponding VBO. These DFT results of MoS_2/HfO_2 interface properties are qualitatively consistent with those obtained from in situ XPS studies of HfO_2 ALD on bulk MoS_2 and highlight the importance of fabricating defect-free interfaces for novel, TMD-based device applications.

4. METHODS AND CALCULATION DETAILS

First-principles calculations are performed on the basis of DFT[51−53] with plane wave basis set and projector-augmented wave pseudopotentials,[54,55] implemented in the Vienna ab initio simulation package.[51,56] The electronic wave functions are represented by plane wave basis with a cutoff energy of 500 eV. The exchange correlation interactions are incorporated as a functional of the GGA.[57−59] Knowing the underestimation of the band gaps obtained from standard GGA calculations, we also used the hybrid functional proposed by Heyd, Scuseria, and Ernzerhof (HSE), in which the short-range part of the exchange functional is represented by a (fixed) combination of GGA and Hartree−Fock contributions, whereas the long-range part and the correlation functional are described by the GGA.[60]

To investigate the MoS_2/HfO_2 interface, an interface model starting with a S-terminated MoS_2 surface and an O-terminated HfO_2 (111) surface, with a lattice mismatch less than 1%, is constructed, as shown in Figure 1a. This interface model contains 5 atomic layers of Hf and 10 atomic layers of O, to minimize the quantum size effects. Although dielectric materials typically become amorphous after annealing at high temperatures to reduce defect formation, the local Hf−O bonding is more important than long-range order for interface engineering. Therefore, the 15 dielectric layers considered represent a good model system for this type of interfaces.[42,43] Periodically repeated slabs are used to model the interface. Each periodic slab is separated by 16 Å of vacuum to avoid interaction between the two surfaces of the slab due to the periodic boundary conditions. In our calculations, the atoms are allowed to relax, whereas the cell size is kept fixed after optimization of the unit cell. A Γ-centered 6 × 6 × 1 k-point within the Monkhorst−Pack scheme[61] mesh is used in the self-consistent field (SCF) calculations, and a 12 × 12 × 1 k-point mesh is used for DOS calculations. An SCF dipole correction is used to cancel spurious electric fields that may be induced by the periodic boundary conditions of the interface model. The energy and forces are converged until tolerance values of 10^{-4} eV and 0.01 eV/Å, respectively.

ASSOCIATED CONTENT

Supporting Information

The Supporting Information is available free of charge on the ACS Publications website at DOI: 10.1021/acsomega.7b00636.

Complete information on the thermodynamic model used to calculate the interface stability, together with the electronic and atomic structures of the different models used to calculate the BOs (PDF)

AUTHOR INFORMATION

Corresponding Authors

*E-mail: roberto.longo@utdallas.edu.
*E-mail: kjcho@utdallas.edu.

ORCID

Santosh KC: 0000-0003-4650-3722
Roberto C. Longo: 0000-0003-4353-841X
Robert M. Wallace: 0000-0001-5566-4806

Notes

The authors declare no competing financial interest.

ACKNOWLEDGMENTS

Calculations were performed in the Texas Advanced Computer Center (TACC). R.M.W. acknowledges discussions with Prof. A. Javey on contact interfaces. This study was supported in part by the Center for Low Energy Systems Technology (LEAST), one of six centers supported by the STARnet phase of the Focus Center Research Program (FCRP), a Semiconductor Research Corporation program sponsored by MARCO and DARPA. This study was also supported by the National Research Foundation of Korea by Creative Materials Discovery Program (2015M3D1A1068062).

REFERENCES

(1) del Alamo, J. A. Nature Insight: Silicon Electronics and Beyond. *Nature* **2011**, *479*, 317−323.
(2) *Fundamentals of III−V Semiconductor MOSFETs*; Oktyabrsky, S., Ye, P. D., Eds.; Springer: New York, 2010.
(3) Hasegawa, H. Fermi Level Pinning and Schottky Barrier Height Control at Metal-Semiconductor Interfaces of InP and Related Materials. *Jpn. J. Appl. Phys.* **1999**, *38*, 1098−1102.
(4) Pasquarello, A.; Hybertsen, M. S.; Car, R. Interface Structure between Silicon and its Oxide by First-Principles Molecular Dynamics. *Nature* **1998**, *396*, 58−60.
(5) Witczak, S. C.; Suehle, J. S.; Gaitan, M. An Experimental Comparison of Measurement Techniques to Extract Si-SiO_2 Interface Trap Density. *Solid-State Electron.* **1992**, *35*, 345−355.
(6) Muller, D. A.; Sorsch, T.; Moccio, S.; Baumann, F. H.; Evans-Lutterodt, K.; Timp, G. The Electronic Structure at the Atomic Scale of Ultrathin Gate Oxides. *Nature* **1999**, *399*, 758−761.
(7) (a) Sandroff, C. J.; Nottenburg, R. N.; Bischoff, J. C.; Bhat, R. Dramatic Enhancement in the Gain of a GaAs/AlGaAs Heterostructure Bipolar Transistor by Surface Chemical Passivation. *Appl. Phys. Lett.* **1987**, *51*, 33−35. (b) Wang, W.; Gong, C.; Xiong, K.; KC, S.; Wallace, R. M.; Cho, K. Materials Design on the Origin of Gap States in a High-κ/GaAs Interface. *Engineering* **2015**, *1* (3), 372−377.
(8) (a) Sandroff, C. J.; Hegde, M. S.; Farrow, L. A.; Chang, C. C.; Harbison, J. P. Electronic Passivation of GaAs Surfaces Through the Formation of Arsenic-Sulfur Bonds. *Appl. Phys. Lett.* **1989**, *54*, 362−364. (b) Qin, X.; Wang, W. E.; Droopad, R.; Rodder, M. S.; Wallace, R. M. A crystalline oxide passivation on $In_{0.53}Ga_{0.47}As$ (100). *J. Appl. Phys.* **2017**, *121*, 125302.

DOI: 10.1021/acsomega.7b00636
ACS Omega 2017, 2, 2827−2834

(9) Novoselov, K. S.; Geim, A. K.; Morozov, S. V.; Jiang, D.; Zhang, Y.; Dubonos, S. V.; Grigorieva, I. V.; Firsov, A. A. Electric Field Effect in Atomically Thin Carbon Films. *Science* **2004**, *306*, 666−669.
(10) Li, X.; Cai, W.; An, J.; Kim, S.; Nah, J.; Yang, D.; Piner, R.; Velamakanni, A.; Jung, I.; Tutuc, E.; Banerjee, S. K.; Colombo, L.; Ruoff, R. S. Large-Area Synthesis of High-Quality and Uniform Graphene Films on Copper Foils. *Science* **2009**, *324*, 1312−1314.
(11) Reina, A.; Jia, X.; Ho, J.; Nezich, D.; Son, H.; Bulovic, V.; Dresselhaus, M. S.; Kong, J. Large Area, Few-Layer Graphene Films on Arbitrary Substrates by Chemical Vapor Deposition. *Nano Lett.* **2008**, *9*, 30−35.
(12) Radisavljevic, B.; Radenovic, A.; Brivio, J.; Giacometti, V.; Kis, A. Single-Layer MoS_2 Transistors. *Nat. Nanotechnol.* **2011**, *6*, 147−150.
(13) Zhou, S. Y.; Gweon, G.-H.; Fedorov, A. V.; First, P. N.; de Heer, W. A.; Lee, D.-H.; Guinea, F.; Neto, A. H. C.; Lanzara, A. Substrate-Induced Bandgap Opening in Epitaxial Graphene. *Nat. Mater.* **2007**, *6*, 770−775.
(14) Williams, J. R.; DiCarlo, L.; Marcus, C. M. Quantum Hall Effect in a Gate-Controlled P-N Junction of Graphene. *Science* **2007**, *317*, 638−641.
(15) Rapoport, L.; Fleischer, N.; Tenne, R. Fullerene-like WS_2 Nanoparticles: Superior Lubricants for Harsh Conditions. *Adv. Mater.* **2003**, *15*, 651−655.
(16) Brown, S.; Musfeldt, J. L.; Mihut, I.; Betts, J. B.; Migliori, A.; Zak, A.; Tenne, R. Bulk vs Nanoscale WS_2: Finite Size Effects and Solid-State Lubrication. *Nano Lett.* **2007**, *7*, 2365−2369.
(17) Onodera, T.; Morita, Y.; Suzuki, A.; Koyama, M.; Tsuboi, H.; Hatakeyama, N.; Endou, A.; Takaba, H.; Kubo, M.; Dassenoy, F.; Minfray, C.; Joly-Pottuz, L.; Martin, J. M.; Miyamoto, A. A Computational Chemistry Study on Friction of H-MoS_2. Part I. Mechanism of Single Sheet Lubrication. *J. Phys. Chem. B* **2009**, *113*, 16526−16536.
(18) Chhowalla, M.; Shin, H. S.; Eda, G.; Li, L. J.; Loh, K. P.; Zhang, H. The Chemistry of Two-Dimensional Layered Transition Metal Dichalcogenide Nanosheets. *Nat. Chem.* **2013**, *5*, 263−275.
(19) Santos, E. J. G.; Kaxiras, E. Electrically Driven Tuning of the Dielectric Constant in MoS_2 Layers. *ACS Nano* **2013**, *7*, 10741−10746.
(20) Ding, Y.; Wang, Y.; Ni, J.; Shi, L.; Shi, S.; Tang, W. First Principles Study of Structural, Vibrational and Electronic Properties of Graphene-Like MX_2 (M = Mo, Nb, W, Ta; X = S, Se, Te) Monolayers. *Physica B* **2011**, *406*, 2254−2260.
(21) Ayari, A.; Cobas, E.; Ogundadegbe, O.; Fuhrer, M. S. Realization and Electrical Characterization of Ultrathin Crystals of Layered Transition-Metal Dichalcogenides. *J. Appl. Phys.* **2007**, *101*, No. 014507.
(22) Morosan, E.; Zandbergen, H. W.; Dennis, B. S.; Bos, J. W. G.; Onose, Y.; Klimczuk, T.; Ramirez, A. P.; Cava, N. P. O. R. J.; et al. Superconductivity in Cu_xTiSe_2. *Nat. Phys.* **2006**, *2*, 544−550.
(23) Hu, W. Z.; Li, G.; Yan, J.; Wen, H. H.; Wu, G.; Chen, X. H.; Wang, N. L. Optical Study of the Charge-Density-Wave Mechanism in 2H-TaS_2 and Na_xTaS_2. *Phys. Rev. B* **2007**, *76*, No. 045103.
(24) Kusmartseva, A. F.; Akrap, A.; Berger, H.; Forro, L.; Tutis, E.; et al. From Mott State to Superconductivity in 1T-TaS_2. *Nat. Mater.* **2008**, *7*, 960−965.
(25) Kam, K. K.; Parkinson, B. A. Detailed Photocurrent Spectroscopy of the Semiconducting Group VIB Transition Metal Dichalcogenides. *J. Phys. Chem.* **1982**, *86*, 463−467.
(26) Han, S. W.; Kwon, H.; Kim, S. K.; Ryu, S.; Yun, W. S.; Kim, D. H.; Hwang, J. H.; Kang, J. S.; Baik, J.; Shin, H. J.; Hong, S. C. Band-Gap Transition Induced by Interlayer van der Waals Interaction in MoS_2. *Phys. Rev. B* **2011**, *84*, No. 045409.
(27) Novoselov, K. S.; Jiang, D.; Schedin, F.; Booth, T. J.; Khotkevich, V. V.; Morozov, S. V.; Geim, A. K. Two-Dimensional Atomic Crystals. *Proc. Natl. Acad. Sci. U.S.A.* **2005**, *102*, 10451−10453.
(28) Coleman, J. N.; et al. Two-Dimensional Nanosheets Produced by Liquid Exfoliation of Layered Materials. *Science* **2011**, *331*, 568−571.
(29) Shi, Y.; Zhou, W.; Lu, A. Y.; Fang, W.; Lee, Y. H.; Hsu, A. L.; Kim, S. M.; Kim, K. K.; Yang, H. Y.; Li, L. J.; Idrobo, J. C.; Kong, J. van der Waals Epitaxy of MoS_2 Layers Using Graphene As Growth Templates. *Nano Lett.* **2012**, *12*, 2784−2791.
(30) Zhan, Y.; Liu, Z.; Najmaei, S.; Ajayan, P. M.; Lou, J. Large-Area Vapor-Phase Growth and Characterization of MoS_2 Atomic Layers on a SiO_2 Substrate. *Small* **2012**, *8*, 966−971.
(31) Eda, G.; Yamaguchi, H.; Voiry, D.; Fujita, T.; Chen, M.; et al. Photoluminescence from Chemically Exfoliated MoS_2. *Nano Lett.* **2011**, *11*, 5111−5116.
(32) Liu, L.; Kumar, S.; Ouyang, Y.; Guo, J. Performance Limits of Monolayer Transition Metal Dichalcogenide Transistors. *IEEE Trans. Electron Devices* **2011**, *58*, 3042−3047.
(33) Yoon, Y.; Ganapathi, K.; Salahuddin, S. How Good Can Monolayer MoS_2 Transistors Be? *Nano Lett.* **2011**, *11*, 3768−3773.
(34) Das, S.; Chen, H.-Y.; Penumatcha, A.; Appenzeller, J. High Performance Multilayer MoS_2 Transistors with Scandium Contacts. *Nano Lett.* **2013**, *13*, 100−105.
(35) Chen, W.; Santos, E. J. G.; Zhu, W.; Kaxiras, E.; Zhang, Z. Tuning the Electronic and Chemical Properties of Monolayer MoS_2 Adsorbed on Transition Metal Substrates. *Nano Lett.* **2013**, *13*, 509−514.
(36) Kang, J.; Liu, W.; Sarkar, D.; Jena, D.; Banerjee, K. Computational Study of Metal Contacts to Monolayer Transition-Metal Dichalcogenide Semiconductors. *Phys. Rev. X* **2014**, *4*, No. 031005.
(37) Jena, D.; Konar, A. Enhancement of Carrier Mobility in Semiconductor Nanostructures by Dielectric Engineering. *Phys. Rev. Lett.* **2007**, *98*, No. 136805.
(38) Chang, J.; Register, L. F.; Banerjee, S. K. Atomistic Full-Band Simulations of Monolayer MoS_2 Transistors. *Appl. Phys. Lett.* **2013**, *103*, No. 223509.
(39) Mishra, V.; Smith, S.; Ganapathi, K.; Salahuddin, S. In *Dependence of Intrinsic Performance of Transition Metal Dichalcogenide Transistors on Materials and Number of Layers at the 5 nm Channel-Length Limit*, IEEE Electron Devices Meeting (IEDM)Technical Digest; IEEE: Washington, DC, 2013; p 139.
(40) McDonnell, S.; Brennan, B.; Azcatl, A.; Lu, N.; Dong, H.; Buie, C.; Kim, J.; Hinkle, C. L.; Kim, M. J.; Wallace, R. M. HfO_2 on MoS_2 by Atomic Layer Deposition: Adsorption Mechanisms and Thickness Scalability. *ACS Nano* **2013**, *7*, 10354−10361.
(41) Anderson, R. L. Germanium-Gallium Arsenide Heterojunctions. *IBM J. Res. Dev.* **1960**, *4*, 283−287.
(42) KC, S.; Dong, H.; Longo, R. C.; Wang, W.; Xiong, K.; Wallace, R. M.; Cho, K. Electronic Properties of InP (001)/HfO_2 (001) Interface: Band Offsets and Oxygen Dependence. *J. Appl. Phys.* **2014**, *115*, No. 023703.
(43) Wang, W.; Xiong, K.; Wallace, R. M.; Cho, K. Impact of Interfacial Oxygen Content on Bonding, Stability, Band Offsets, and Interface States of GaAs:HfO_2 Interfaces. *J. Phys. Chem. C* **2010**, *114*, 22610−22618.
(44) Addou, R.; Colombo, L.; Wallace, R. M. Surface Defects on Natural MoS_2. *ACS Appl. Mater. Interfaces* **2015**, *7*, 11921−11929.
(45) Addou, R.; McDonnell, S.; Barrera, D.; Guo, Z.; Azcatl, A.; Wang, J.; Zhu, H.; Hinkle, C. L.; Quevedo-Lopez, M.; Alshareef, H. N.; Colombo, L.; Hsu, J. W. P.; Wallace, R. M. Impurities and Electronic Property Variations of Natural Mo_2 Crystal Surfaces. *ACS Nano* **2015**, *9*, 9124−9133.
(46) Thakur, P.; Cezar, J. C.; Brookes, N. B.; Choudhary, R. J.; Prakash, R.; Phase, D. M.; Chae, K. H.; Kumar, R. Direct Observation of Oxygen Induced Room Temperature Ferromagnetism in MoO_2 thin Films by X-Ray Magnetic Circular Dichroism Characterizations. *Appl. Phys. Lett.* **2009**, *94*, No. 062501.
(47) Chuang, S.; Battaglia, C.; Azcatl, A.; McDonnell, S.; Fang, H.; Kang, L.; Yin, X.; Tosun, M.; Kapadia, R.; Wallace, R. M.; Javey, A. MoS_2 P-type Transistors and Diodes Enabled by High Work Function MoO_x Contacts. *Nano Lett.* **2014**, *14*, 1337−1342.

DOI: 10.1021/acsomega.7b00636
ACS Omega 2017, 2, 2827−2834

(48) KC, S.; Longo, R. C.; Addou, R.; Wallace, R. M.; Cho, K. Impact of Intrinsic Atomic Defects on the Electronic Structure of MoS_2 Monolayers. *Nanotechnology* **2014**, *25*, No. 375703.
(49) Santosh, K. C.; Longo, R. C.; Wallace, K.; Cho, K.; et al. Electronic Properties of MoS_2/MoO_x Interfaces: Implications in Tunnel Field Effect Transistors and Hole Contacts. *Sci. Rep.* **2016**, *6*, No. 33562.
(50) Hinkle, C. L.; Sonnet, A. M.; Vogel, E. M.; McDonnell, S.; Hughes, G. J.; Milojevic, M.; Lee, B.; Aguirre-Tostado, F. S.; Cho, K.; Kim, J.; Wallace, R. M. Frequency Dispersion Reduction and Bond Conversion on *N*-Type GaAs by *In Situ* Surface Oxide Removal and Passivation. *Appl. Phys. Lett.* **2007**, *91*, No. 163512.
(51) Kresse, G.; Furthmüller, J. Efficiency of Ab Initio Total Energy Calculations for Metals and Semiconductors Using a Plane-Wave Basis Set. *Comput. Mater. Sci.* **1996**, *6*, 15−50.
(52) Parr, R. G.; Yang, W. *Density-Functional Theory of Atoms and Molecules*; Oxford University Press: New York, 1989.
(53) Kohn, W.; Sham, L. J. Self-Consistent Equations Including Exchange and Correlation Effects. *Phys. Rev.* **1965**, *140*, A1133−A1138.
(54) Kresse, G.; Joubert, D. From Ultrasoft Pseudopotentials to the Projector Augmented-Wave Method. *Phys. Rev. B* **1999**, *59*, 1758−1775.
(55) Blöchl, P. E. Projector Augmented-Wave Method. *Phys. Rev. B* **1994**, *50*, 17953−17979.
(56) Kresse, G.; Hafner, J. Ab Initio Molecular Dynamics for Liquid Metals. *Phys. Rev. B* **1993**, *47*, 558−561.
(57) Kresse, G.; Furthmüller, J. Efficient Iterative Schemes for Ab Initio Total-Energy Calculations Using a Plane-Wave Basis Set. *Phys. Rev. B* **1996**, *54*, 11169−11186.
(58) Kresse, G.; Hafner, J. Ab Initio Molecular-Dynamics Simulation of the Liquid-Metal-Amorphous-Semiconductor Transition in Germanium. *Phys. Rev. B* **1994**, *49*, 14251−14269.
(59) Perdew, J. P.; Burke, K.; Ernzerhof, M. Generalized Gradient Approximation Made Simple. *Phys. Rev. Lett.* **1996**, *77*, 3865−3868.
(60) Heyd, J.; Scuseria, G. E.; Ernzerhof, M. Hybrid Functionals Based on a Screened Coulomb Potential. *J. Chem. Phys.* **2003**, *118*, 8207−8215.
(61) Monkhorst, H. J.; Pack, J. D. Special Points for Brillouin-Zone Integrations. *Phys. Rev. B* **1976**, *13*, 5188−5192.

DOI: 10.1021/acsomega.7b00636
ACS Omega 2017, 2, 2827−2834